Journal of Building Engineering 18 (2018) 84–94

Contents lists available at ScienceDirect

Journal of Building Engineering

journal homepage: www.elsevier.com/locate/jobe

# Torsional behavior of T- shaped reinforced concrete beams with large web openings☆

Ahmed E. Salama[a], Magdy E. Kassem[b], Ahmed A. Mahmoud[c,*]

[a] Cairo University, Cairo
[b] Prof. of RC, Cairo University, Cairo
[c] Prof. of RC, Benha University, Shoubra, Cairo

ARTICLE INFO

*Keywords:*
Reinforced concrete
T- shaped RC beams
Pure torsion
Web opening
Softened truss model

ABSTRACT

This paper presents the results of an experimental investigation on the behavior of T- shaped RC beams with rectangular web opening under pure torsion. Seven beam specimens were tested in order to study the influence of geometrical parameters on the torsional strength. The investigated parameters were: (1) the flange width, (2) the flange thickness, and (3) the opening height. All specimens had the same span, same depth, same web width and same opening length. All beams were loaded till failure. Cracking patterns were monitored and systematic measurements were taken to draw the torque-angle of rotation curves. The results are analyzed to study the effects of the studied parameters on the cracking torque, the ultimate torque, the angle of rotation at cracking, the angle of rotation at ultimate, and failure modes. The analysis of testing results highlights several key aspects to provide a set of recommendations for such beams. The experimental results show that the geometrical parameters (flange width, flange height, and opening height) have a profound effect on the behavior of T-shaped RC beams under pure torsion. A new analytical model based on softened truss model has been used for predicting the torsional behavior of the tested beams. The softened truss model has been successively used for torsion, which is extended to T-shaped RC beams with large web opening under pure torsion. The analytical torque-rotation curves were compared with the experimental ones and observations were noted.

## 1. Introduction

The need of openings in structural elements is common to pass ducts of mechanical and electrical services. The effect of the web opening on the beam strength and service capability must be taken into consideration. This effect depends on opening positions, shapes, and dimensions. Generally, openings are not located closer than one-half of the beam's depth to the supports to avoid the critical region for shear failure and reinforcement congestion [1].

Common opening shapes in reinforced concrete beams are circular and rectangular. Other shapes of opening such as square, triangular, diamond or irregular can also be made. The common size classification expressions are "large openings" and "small openings". This classification is important since the behavior of reinforced concrete beams with openings depends on the opening size. The analysis theories and design methods of beams with small openings differ from those with large openings. In the earlier studies, researchers used these expressions to distinguish between the two types of openings but without an exact definition for each. Mansur et al. [2] and Abul Hasnat et al. [3] suggested that the opening is large if the opening length is greater than the height of either the top chord or the bottom chord, and is small otherwise.

The extensive studies carried out on beams with web opening focused on the effect of opening on beam strength, behavior, and to create a suitable method of design [1–7]. Valuable investigations on the behavior of angular, rectangular and T-shaped RC beams under pure torsion, under combined shear and torsion, pure shear, pure bending moment, pure torsion, combined shear and bending moment or combined bending moment and torsion were made by several researchers [8–18]. However, most of these studies focused on rectangular beams rather than T-shaped beams.

In recent years, efforts have been devoted to experimental investigations and theoretical models have been developed for creating suitable method of design for reinforced concrete torsional members [6,15,19–22]. Nevertheless, the international codes as ACI code [23], Canadian code [24] and the Egyptian code of building [25] do not give any recommendations for analyzing or designing reinforced concrete T-shaped RC beams with web opening under pure torsion. Limited

☆ This research did not receive any specific grant from funding agencies in the public, commercial, or not-for-profit sectors.
* Corresponding author.
*E-mail addresses:* eng.ahmedsalem9@gmail.com (A.E. Salama), magdykassem@feng.cu.edu.eg (M.E. Kassem), ahmed.ahmed@feng.bu.edu.eg (A.A. Mahmoud).

https://doi.org/10.1016/j.jobe.2018.02.004
Received 4 January 2016; Received in revised form 6 July 2017; Accepted 5 February 2018
Available online 09 February 2018

research on the behavior of normal and high strength rectangular RC beams with web opening under pure torsion exists in the literature [2–4,6,7]. El-Badry [7] studied experimentally and theoretically the behavior of high strength rectangular RC beams under pure torsion. The variables were the concrete strength, opening height to section depth ratio, opening depth to its length ratio and opening vertical eccentricity. El-Badry [7] proposed a theoretical model to calculate torsion capacity, the corresponding rotation angle in all stages of loading until failure and failure occur by formation of two diagonal cracks through the opening opposite corners. Another study by Abd EL Salam [4] investigated experimentally the behavior of normal strength RC beams under pure torsion for a rectangular section. The studied variables were ratio of opening width to the beam depth, ratio of opening depth to the beam depth, ratio of the horizontal eccentricity of the opening along beam axis to the beam depth, amount of longitudinal reinforcement at the top and the bottom, spacing between stirrups above and below the opening and details of reinforcement around the opening. Deifalla and Ghobarah [8,10], developed and implemented an innovative test setup capable of simulating the behavior of inverted T-shaped RC beams under combined shear and torsion. The behavior of three inverted T-shaped RC beams tested under different values for the ratios of the applied torque to the applied shear force. In addition, Deifalla et al [26–28], studied the analysis and design of strengthening T-shaped beams using Fiber Reinforced Polymer (FRP) laminates subjected to torsion

In this paper, the experimental results of seven beam specimens are presented and discussed clearly for each studied parameter to investigate the influence of various geometrical parameters on the torsion strength of T- shaped RC beams with web opening. The primary objective of this research is to study the effect of flange width, flange thickness, and opening height on the ultimate torsional moment capacity, and angle of rotation - torque relationships. In addition, the nonlinear behavior of the tested beams was compared with the predicted torque-rotation curves using a new analytical model which was proposed by the authors. The verification of the proposed analytical model was achieved by comparing the predicted and experimental behavior of the seven T-shaped RC beams which were tested by the authors. The predicted torque – rotation curves show good agreement compared with the experimental ones.

## 2. Test program description

### 2.1. Test specimens

The experimental program consisted of seven T- shaped RC beams. The total length of each specimen was taken 1700 mm, and the overall length of the beam was divided into three parts. The middle part with 1300 mm length was the tested zone. The end parts were heavily reinforced concrete cantilevers to prevent premature failure during testing. Table 1 shows the main parameters of the tested specimens. The specimens were designed according to the Egyptian code 2009 [25]. The dimensions of web width and depth were constant and taken as 200 mm x 400 mm. The openings were concentric with respect to the beam depth. The dimensions and steel details for the tested beams are shown in Fig. 1 in elevation and cross section. Closed stirrups of 10 mm diameter were used with 200 mm spacing along the beam span. To study the effect of geometrical parameters (flange thickness and opening height), the tested beams were divided into three groups, in addition to the control specimen $B_1$ without opening. The first group consisted of three beams; $B_2$, $B_3$, and $B_4$, where the flange width was 600 mm, 800 mm and 1000 mm respectively. For the second group, the three beams were $B_5$, $B_3$, and $B_6$ where the flange thicknesses were 100 mm, 120 mm and 150 mm respectively. For the first and second group, the depth of the openings was 60 mm which represents 15% of the beam depth. The third group composed of beams, $B_3$, and $B_7$ with opening depths 60 mm and 120 mm which corresponds to 15% and 30% reduction in the cross-sectional area of the beam.

### 2.2. Material properties

For all specimens, the normal-strength concrete mix was designed to develop a characteristic compressive strength of 30 MPa after 28 days. The concrete mix consisted of 1240 kg of coarse aggregate, 620 kg of fine aggregate, 350 kg cement, 180 l of water per 1.0 $m^3$ of concrete. The compressive strength was determined using standard cubes (150 × 150 × 150 mm) at 7 days, 28 days and the day of testing. All beams were cured by water sprinkling for 28 days and then left in the laboratory atmosphere till testing day. Foam blocks were inserted in the beams with the required opening dimensions to form openings. Longitudinal steel reinforcement of 12 mm diameter and closed stirrups of 10 mm diameter have yield strength 384 MPa was used. In addition to the closed stirrups, 8 mm diameter with yield strength 248 MPa was used in the loading cantilever. Fig. 2a shows the geometry of the steel reinforcement of some tested beams during constructing. Fig. 2b shows some tested beams after casting.

### 2.3. Test setup

The test set-up was constructed to apply a pure torsional moment to the tested specimens; where test specimens were simply supported on movable supports as shown in Fig. 3c. During the test operation, the specimens were subjected to vertical load by a hydraulic jack of 1000 kN-capacity attached to a rigid steel frame. A sensitive load cell was used to measure the vertical load. The applied vertical load was equally distributed on both cantilevers by rigid steel I-beam as shown in Fig. 3b. Two Linear Variable Displacements Transducers (LVDTS) were attached to the two ends of the cantilevers to measure the vertical displacement at various loading stages. All the instrumentations were

**Table 1**
Details of the tested specimens.

| Beam specimen | B (mm) | $t_s$ (mm) | $h_o$ (mm) | $L_o$ (mm) | $t_t$ (mm) | $t_b$ (mm) | A ($mm^2$) | $\rho_l$ (%) | $\rho_t$ (%) | ($\rho_t$/ $\rho_l$) |
|---|---|---|---|---|---|---|---|---|---|---|
| $B_1$ | 800 | 120 | 0 | 0 | 0 | 0 | 152,000 | 0.743 | 0.258 | 0.347 |
| $B_2$ | 600 | 120 | 60 | 600 | 170 | 230 | 128,000 | 1.236 | 0.307 | 0.248 |
| $B_3$ | 800 | 120 | 60 | 600 | 170 | 230 | 152,000 | 1.041 | 0.258 | 0.248 |
| $B_4$ | 1000 | 120 | 60 | 600 | 170 | 230 | 176,000 | 0.899 | 0.223 | 0.248 |
| $B_5$ | 800 | 100 | 60 | 600 | 170 | 230 | 140,000 | 1.130 | 0.280 | 0.248 |
| $B_6$ | 800 | 150 | 60 | 600 | 170 | 230 | 170,000 | 0.931 | 0.231 | 0.248 |
| $B_7$ | 800 | 120 | 120 | 600 | 140 | 260 | 152,000 | 1.041 | 0.258 | 0.248 |

Where, B is the flange width; $t_s$ is the flange thickness; $h_o$ is the depth of the opening; $L_o$ is the length of the opening; $t_t$ is the distance measured from the top face of the beam to the top of the opening; $t_b$ is the distance measured from the bottom face of the beam to the bottom of the opening; A is the gross cross sectional area; $\rho_l$ is the ratio of the longitudinal reinforcement area to the gross cross section area of the RC section; and $\rho_l$ is the ratio of the transversal reinforcement area to the gross cross section area of the RC section.

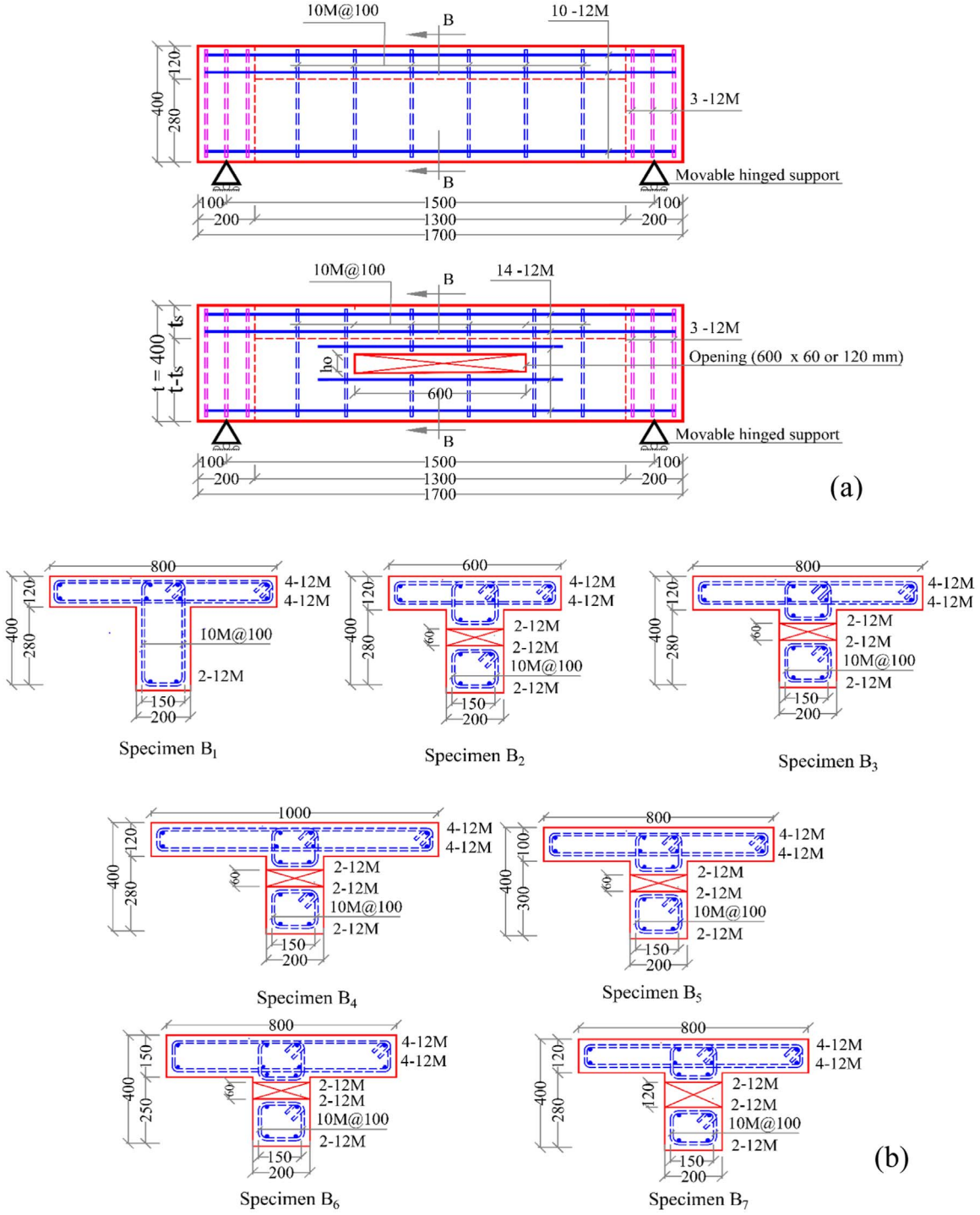


**Fig. 1.** Dimensions and details for all tested specimens (a) Typical elevations for control specimen and specimens with openings (b) Cross sections for all tested specimens.

connected to a data acquisition system (DAQ) to record the readings during the test.

The load on each cantilever was applied in increments. About 15 load increments were used up to failure. After each increment, the readings of vertical load and vertical displacement were recorded. The development and propagation of cracks were marked up to failure. The rotation angle was measured by dividing the deflections under both two loaded points by the distance between the centerline of the tested beams and the loaded point. The torque measured by multiplying the applied load on the cantilever by the distance between the centerline of tested beams and the loaded point.

## 3. Test results and discussion

### 3.1. Cracking patterns and failure modes

The cracking patterns in the vertical and the horizontal faces for each beam under pure torsion are shown in Fig. 4. The crack pattern is nearly the same for all beams. The first crack appeared at the corner of the opening. These cracks were inclined with approximately 45 degrees' angle to the longitudinal axis of the beam. The angle of inclination of the compression diagonals with respect to the beam axis, θ, depends on the ratio of the force carried by the longitudinal reinforcement to that


**Fig. 2.** Test specimens (a) reinforcement and (b) after casting.

carried by the stirrups [29]. There are many cracks appeared on the vertical and outer horizontal faces especially at the bottom chord of each beam. These cracks at the inside horizontal face of the top and the bottom chords occurred at the later stage of loading especially at the top chord due to the existence of the slab which resists the applied torsional moment. The cracks were spirally trajectory on the four sides of tested beams due to shear stresses from torsion. The crushing of concrete was the main cause of the failure mode in all the tested beams. The crushing zones were in the solid section and were joined by spiral-diagonal tension cracks around the remaining three beam faces. Fig. 5 shows the cracking patterns of the tested specimens at failure. The ratio of the transversal and longitudinal reinforcement as shown in Table 1, strongly governs the ratio of the forces carried by the longitudinal and transversal reinforcement which can be seen in the global failure mode as well as the angle of the cracks in the ultimate state.

### 3.2. Torque - rotation curves

Fig. 6 shows the effect of flange width, flange thickness and opening height on the measured torque – rotation curves respectively. These curves show that the relation between the applied torsional moment and the angle of rotation can be divided into two main parts. The first

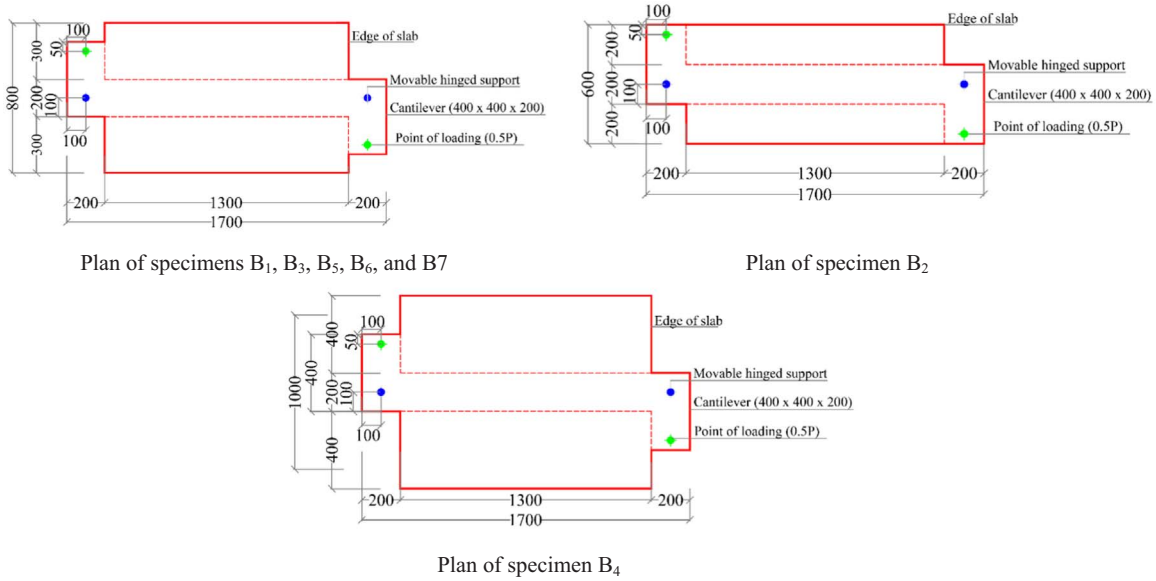


Plan of specimens $B_1$, $B_3$, $B_5$, $B_6$, and B7

Plan of specimen $B_2$

Plan of specimen $B_4$

(a) Plans of the tested specimen

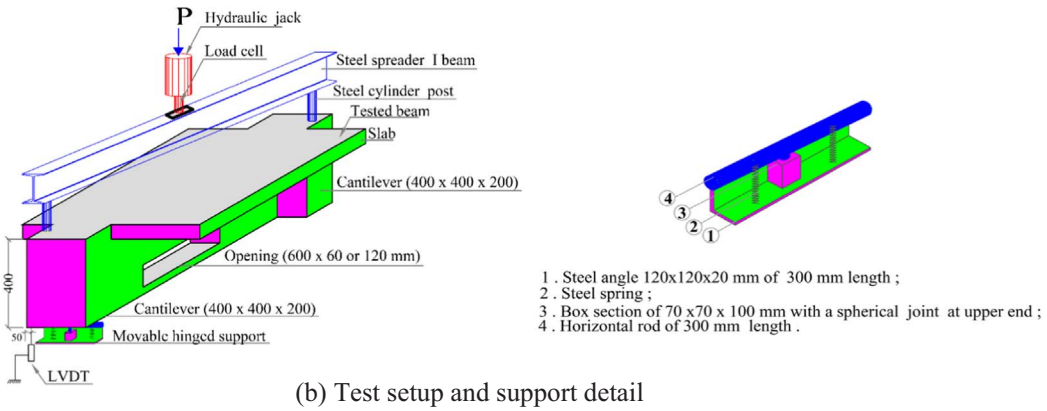


(b) Test setup and support detail

**Fig. 3.** Arrangement of the test setup.


**Fig. 4.** Cracking patterns of the tested specimens in horizontal and vertical faces.

part is linear up to the cracking torque. The second part is nonlinear and the slope of the curve decreases with increasing the torque indicating the post-cracking behavior. All tests were performed under load control; therefore, the torque-rotation curves do not incorporate a descending branch after the maximum torque. Therefore, torque-rotation curves do not allow concluding the influence of the studied variables on the ductility of the studied beams.

### *3.3. Measured torque and rotation angle at working and ultimate levels*

The measured torque and rotation angle at working and ultimate levels are summarized in Table 2 for each specimen. The effect of flange width on the measured results for beams ($B_2$, $B_3$, and $B_4$) are shown in Fig. 7a. The cracking torque is increased for beams $B_3$ (with B = 800 mm) and $B_4$ (with B = 1000 mm) by about 12% and 22% respectively, compared to the cracking torque of beam $B_2$ (with B = 600 mm) while the ultimate torque is increased by about 4% and 10% respectively. On the other hand, the cracking angle of rotation is increased for beams $B_3$ and $B_4$ by about 29% and 43% respectively, compared to the cracking angle of rotation of beam $B_2$. The angle of rotation at ultimate is increased by about 25% and 29% respectively. It is clear that the measured torque and rotation angle at cracking and ultimate levels are increased with the increase of flange width.

Fig. 7.b shows the effect of flange thickness on the cracking and the ultimate torque for the three tested beams ($B_3$, $B_5$, and $B_6$). The figure indicates that the increase of flange thickness increases the cracking and the ultimate torques. The cracking torque is increased for beam $B_3$ (with $t_s$ = 120 mm) and $B_6$ (with $t_s$ = 150 mm) by about 53% and 108% respectively, compared to the cracking torque of beam $B_5$ (with $t_s$ = 100 mm) while the ultimate torque is increased by about 5% and 33% respectively. The angle of rotation at the first crack is increased for beam $B_3$ and beam $B_6$ by about 50% and 83% respectively compared to

(a) Failure mode of beam specimen $B_1$ and $B_2$

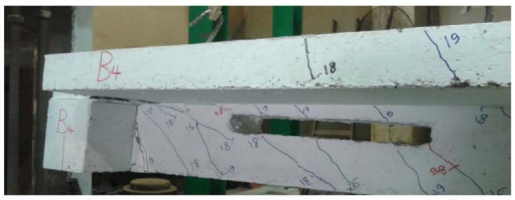

(b) Failure mode of beam specimen $B_3$ and $B_4$

(c) Failure mode of beam specimen $B_5$ and $B_6$

(d) Failure mode of beam specimen B7

**Fig. 5.** Cracking patterns of the tested specimens at failure.

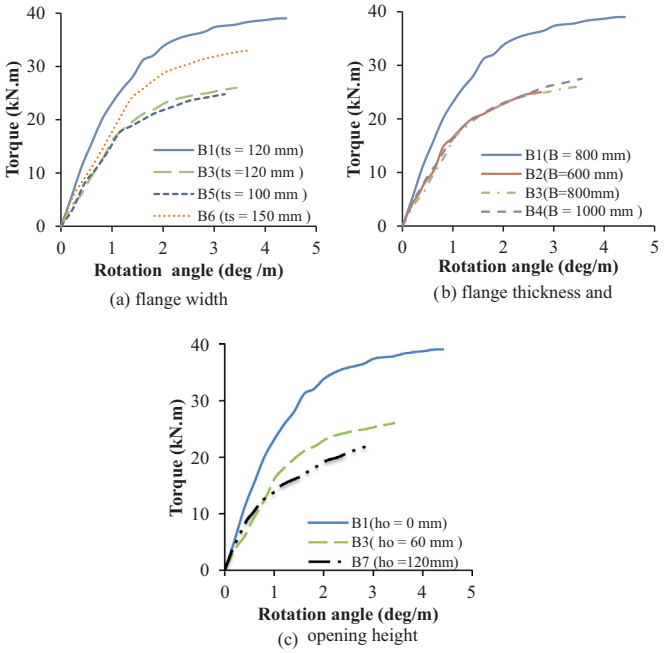


**Fig. 6.** Torque - rotation curves show the effect of (a) flange width (b) flange thickness and (c) opening height.

**Table 2**
Experimental results of the tested specimens.

| Beam specimen | $T_{cr}$ (kN. m) | $\theta_{cr}$ (deg/ m) | $T_u$ (kN.m) | $\theta_u$ (deg/m) | Tcr / Tu (%) | $\theta_{cr}$ (%) |
|---|---|---|---|---|---|---|
| $B_1$ | 28.0 | 1.403 | 39 | 4.41 | 71.79 | 31.81 |
| $B_2$ | 14.7 | 0.80 | 25 | 2.75 | 58.80 | 29.00 |
| $B_3$ | 16.5 | 1.03 | 26 | 3.44 | 63.46 | 29.94 |
| $B_4$ | 18 | 1.15 | 27.5 | 3.55 | 65.45 | 32.39 |
| $B_5$ | 10.8 | 0.69 | 24.8 | 3.2 | 43.55 | 21.56 |
| $B_6$ | 22.5 | 1.26 | 33 | 3.67 | 68.18 | 34.33 |
| $B_7$ | 10.2 | 0.57 | 21.9 | 2.86 | 46.58 | 19.93 |

where, $T_{cr}$ is the cracking torque; $\theta_{cr}$ is the angle of rotation at first crack; $T_u$ is the ultimate torque;and $\theta_u$ is the angle of rotation at ultimate.

the angle of rotation at cracking of beam $B_5$. The angle of rotation at ultimate is increased by about 7% and 14% respectively. It is obvious that the increase of flange thickness ($t_s$) increases the cracking torque, ultimate torque and corresponding angles of rotation.

The cracking and ultimate torque for the three tested beams ($B_1$, $B_3$, and $B_7$) with different opening height is shown in Fig. 7c. The cracking torque is decreased for beam $B_3$ (with $h_o$ = 60 mm) and beam $B_7$ (with $h_o$ = 120 mm) by about 41% and 64% respectively compared to cracking torque of beam $B_1$ without opening. The ultimate torque is decreased by about 33% and 44% respectively. The angle of rotation at the first crack is decreased for beams $B_3$ and $B_7$ by about 27% and 59% respectively compared to the angle of rotation at cracking of beam $B_1$ without opening, the angle of rotation at ultimate is decreased by about

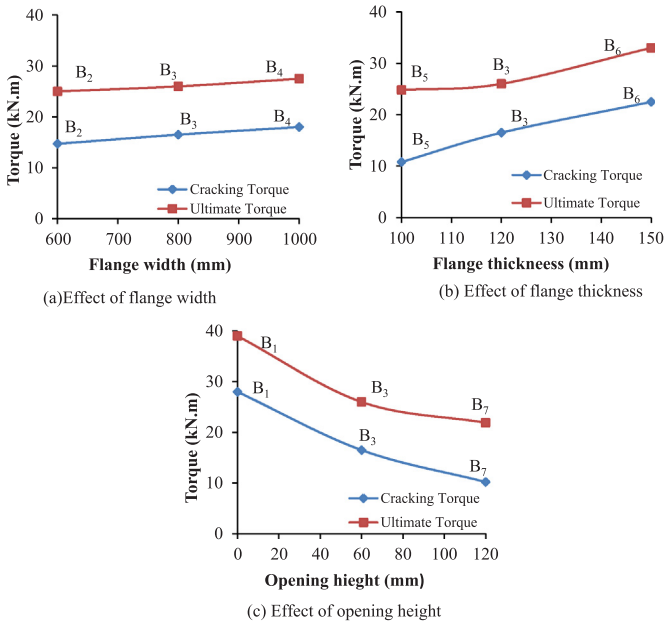


**Fig. 7.** Cracking and ultimate torque versus flange width, flange thickness and opening height.

22% and 35% respectively. It indicates that the increase of opening height ($h_o$) decreases the cracking torque, ultimate torque and the corresponding angle of rotation at the first crack and at the ultimate.

## 4. The proposed analytical model

The torsional strength of members with both longitudinal steel and stirrups is determined by two different elastic analysis methods, which are skew bending theory [30] and space truss model theory. The space truss model theory is divided into Rausch truss analogy [12] and the variable angle truss model [31]. When a beam is subjected to pure torsion its cross section is idealized as a thin-walled tube and the concrete core is neglected as shown in Fig. 8. After cracking the torsional strength is provided by closed stirrups and longitudinal bars. The beam will resist the torsional moment by the outer side perimeter of the beam section and the concrete will be separated into series of diagonal concrete struts at an angle (θ) [29]. Thus, truss model theory considers all sections; hollow or solid sections are idealized as thin-walled tubes after cracking. The torsional moment acts as a shear force on the outside perimeter of the beam section. Each edge of the beam section is resisting this shear force as a plane truss model which represents separate beam with width ($t_e$) as shown in Fig. 8. Therefore, the beam is resisting this torsional moment by four plane trusses at each edge forming what is known as space truss model.

The space truss model consists of longitudinal reinforcement representing the top and the bottom chords of the truss; closed stirrups representing the vertical members of the truss; and diagonal concrete compression members between spiral cracks around the beam representing the diagonal members of the truss. Fig. 9 shows the components of space truss model. The space truss model is included in the latest versions of the ACI 318–14 [23]. Therefore, for any beam either solid or hollow, the external fibres of the beam only contribute in resisting torsional moment. Thin walled section analysis used to predict the shear stresses due to torsion in hollow section as well as in solid sections.

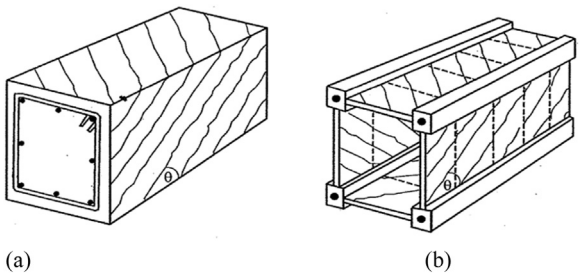


**Fig. 8.** The idealized cross section for torsion (a) Section of the actual beam (b) Truss model ideal section [29].

Rausch [12] extended Morsch 45° truss model [32] for design shear and torsion and derived an equation to predict torsional strength of solid reinforced concrete members based on space truss model but it overestimates the actual torsional strength of any members. The softening of concrete due to diagonal cracking causes the un-conservative nature of Rausch's equation [12]. Consequently, using a new stress-strain curve for softened concrete improved the prediction of torsional strength. The applied moment is resisted by a field of diagonal compressive stresses in the concrete strut, which does not exceed cylinder compressive strength due to the existence of transverse tensile strain. This phenomenon is called "concrete softening in compression". Numerous models for softened stress strain curve proposed by Vecchio and Collins were found in existing literature [33–36]. In the present analysis, the softening concrete parameter (β) is calculated based on the modified compression field theory [35] that is provided by Canadian code (CAN/CSA A 23.3–14) [24]. A new analytical model was developed and an analytical procedure was proposed for nonlinear analysis of T-shaped RC beams with large web opening subjected to pure torsion to calculate torque and angle of rotation at all stages of loading where the behavior of T-shaped RC beams under torsion is studied by means of torque – rotation curves. The analytical method employs the combination of model of concrete softening and space truss model. The softened truss model has been successively used for torsion, which is extended to T-shaped RC beams with large web opening under pure torsion. The nonlinear behavior for the materials (concrete and steel reinforcement) is incorporated by mean of stress (σ)-strain ($\varepsilon_0$) relationships. The verification of the proposed analytical model is achieved through extensive comparisons between torque-rotation curves that are obtained from current analytical model and the experimental results of the seven beams that were tested by the authors.

### 4.1. Analysis of the proposed analytical model

The proposed analytical model in this study based on the developing of the softened truss model proposed by Hsu et al. [21] which depends on an iterative analysis procedure for sections analysis subjected to pure torque. The softened space truss model, developed by Hsu, is similar to the space truss model described above; except that it utilizes the full concrete cross section and takes concrete softening into consideration. The model was developed according to the fundamental principles of the mechanics of materials, stress equilibrium, strain compatibility, and the constitutive law of materials. The used analytical procedure is proposed with several simplifications by assuming the angle of inclination of the diagonal concrete struts (θ) equals 45 degrees for non-pre-stressed reinforced concrete members [23]. The softening concrete parameter is calculated from Eq. (13) [24] and the equivalent thickness of shear flow zone ($t_e$) is calculated from ACI equation [23]. The modified model is extended to analyze T-shaped RC concrete beams with large web opening under pure torsion. The analysis procedure is applied by dividing the beam into two parts, top and bottom chords. The top chord is the T-shaped part above the opening and the bottom chord is the rectangular part below the opening (Fig. 10). The sum of the torsional moments for the top and bottom chords is the total moment applied on the beam and the angle of rotation assumed to be the maximum angle of the two parts. However, for the T-shaped RC beams without openings the beam is considered as a top chord with depth equals the total depth of the beam and the depth of the bottom chord equals zero.

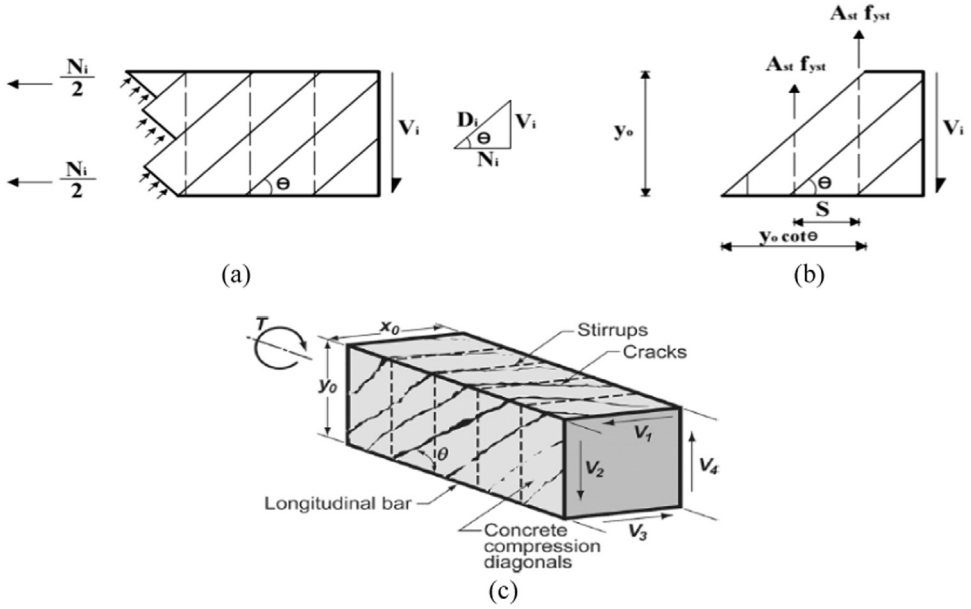


**Fig. 9.** Space truss model (a) Resolution of shear force $V_i$ into diagonal compression force $D_i$ and axial tension force Ni (b) force in the stirrups (C) components of idealized space truss model [23].

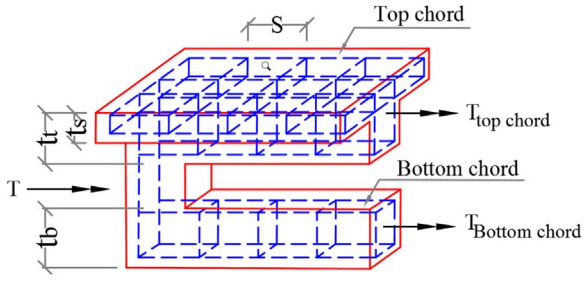


**Fig. 10.** Definition of top and bottom chords in T-shaped beam with opening.

The analysis of the proposed model can be summarized in the following points briefly:

1st: Determine the shear stress due to torsion in each face of the beam where each face acts as a beam with width ($t_e$) resists a shear stress $\tau$ by plane truss. The shear flow (q) is the product of shear stress ($\tau$) by the equivalent thickness of shear flow zone ($t_e$) with constant value at all points around the perimeter of the tube. The shear flow path acts at mid-thickness of the walls of the tube, as shown in Fig. 9b. The shear stress due to torsion at any point along the perimeter of the tube can be calculated from Eq. (1). the equivalent thickness of shear flow zone ($t_e$) can be calculated from Eq. (8). The cross-section properties ($A_o$) and ($A_{oh}$) are expressed by the shaded areas (Fig. 11). The cross-section properties can be calculated for the rectangular and T-shaped sections from Eqs. (2)–(6), respectively.

$$\tau = \frac{T}{2A_o t_e} \tag{1}$$

- For rectangular section:

$$A_{oh} = (b - 2d`)(t - 2d`) \tag{2}$$

$$A_o = (b - t_e)(t - t_e) \cong 0.85A_{oh} \tag{3}$$

$$P_h = 2[(b - 2d`) + (t - 2d`)] \tag{4}$$

- For T- shaped section:

$$A_{oh} = [(B - 2d`)(t_s - 2d`) + (b - 2d`)(t - t_s - d`)] \tag{5}$$

$$A_o = [(B - t_e)(t_s - t_e) + (b - t_e)(t - t_s - 0.5t_e)] \cong 0.85A_{oh} \tag{6}$$

$$P_h = 2[(B - 2d`) + (t - 2d`)] \tag{7}$$

$$t_e = \frac{A_{oh}}{P_h} \tag{8}$$

Where, ($A_o$) the area enclosed by the centerline of the shear flow zone equals 0 .$85A_{oh}$ (ACI 318–14); ($A_{oh}$) is the gross area bounded by the

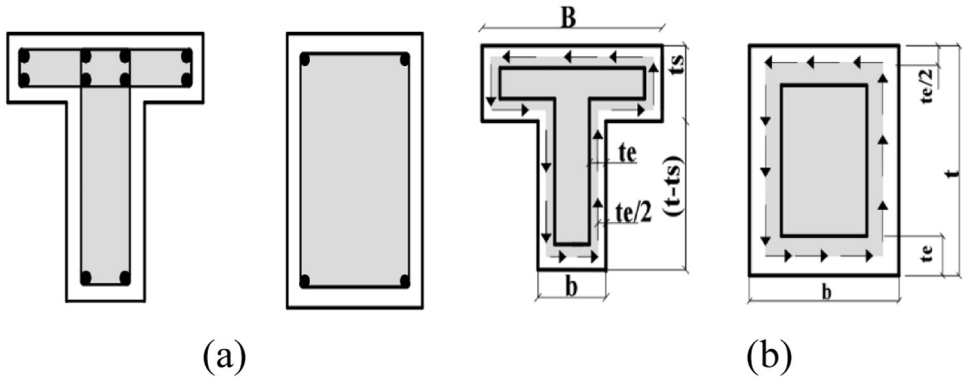


**Fig. 11.** Definition of $A_o$, $A_{oh}$ and $P_h$ for rectangular and T- shaped beam cross section (a) Area and perimeter enclosed by the centerline of stirrups ($A_{oh}$),($P_h$) (b) Area enclosed by shear flow path ($A_o$).

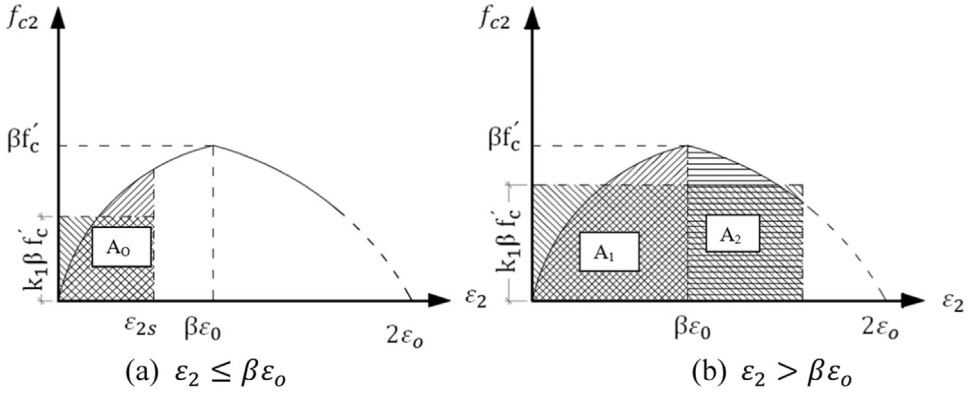


**Fig. 12.** Stress-strain curve for softened concrete [35].

centerline of the outer most closed stirrups and ($P_h$) is the perimeter of the closed stirrup.

2nd: Study equilibrium for each face of the space truss to calculate the internal forces in each plane truss. Fig. 9a shows the analysis of one face of the space truss where the shear force $V_i$ is resolved into a diagonal compressive force ($D_i = V_i / \sin\theta$) and an axial tension force $N_i$. The force $D_i$ is resisted by compressive stress in the struts. The diagonal compressive strength acting on the softened concrete struts can be given by:

$$f_{cd} = \frac{T}{2\ A_o t_e \sin\theta\cos\theta} \tag{9}$$

So, the torsional moment equals

$$T = 2A_o t_e f_{cd} \sin\theta\cos\theta \tag{10}$$

3rd: The stress-strain curve for softened concrete is used in the current theoretical model that was proposed by Vecchio and Collins [35] as shown in Fig. 12. The curve is divided into two regions:

Region 1: For $\varepsilon_2 \le \beta\varepsilon_o$, the equation of ascending portion of the curve is:

$$f_{c2} = f_c^{'}\left[2\left(\frac{\varepsilon_2}{\varepsilon_0}\right) - \frac{1}{\beta}\left(\frac{\varepsilon_2}{\varepsilon_o}\right)^2\right] \tag{11}$$

Region 2: For $\varepsilon_2 > \beta\varepsilon_o$ the equation of the descending portion of the curve is:

$$f_{c2} = \beta f_c^{'}\left[1 - \left(\frac{\varepsilon_2 - \varepsilon_p}{2\varepsilon_0 - \varepsilon_p}\right)^2\right] \tag{12}$$

Where $\varepsilon_p = \beta\ \varepsilon_0$

(a) $\varepsilon_2 \le \beta\varepsilon_o$ (b) $\varepsilon_2 > \beta\varepsilon_o$

The average compressive stress for the softened concrete struts in the space truss model ($f_{cd}$ ), which is related to the maximum compressive stress $\beta f_c^{`}$ is computed by using equation (15). The factor $k_1$ is the ratio of the average stress ($f_{cd}$) to peak stress ($\beta f_c^{`}$) and can be calculated by integration of stress – strain curve equations in Fig. 12 as expressed in Eqs. (16) and (17), or can be obtained from Table 1 [21] as a function of the concrete compressive strain at concrete surface ($\varepsilon_{2\,s}$) and the softening parameter (β). The parameter β can be calculated from Eq. (13) according to Canadian code equation (CAN/CSA A 23.3–14) [24].

$$\beta = \frac{1}{0.8 + 170\,\varepsilon_1} \tag{13}$$

$$\varepsilon_1 = \varepsilon_l + (\varepsilon_l + 0.002)cot^2\,\theta \tag{14}$$

$$f_{cd} = k_1\beta f_c^{`}\ \text{so},\ k_1 = \frac{f_{cd}}{\beta f_c^{`}} = \frac{\text{average stress}}{\text{peak strenght}} \tag{15}$$

For $\varepsilon_{2S} \le \beta\varepsilon_O$

$$K_1\beta f_c^{`} = \frac{A_o}{\varepsilon_{2s}} = \frac{1}{\varepsilon_{2s}}\int_0^{\varepsilon_{2S}} \beta f_c^{'}\left[2\left(\frac{\varepsilon_2}{\varepsilon_p}\right) - \left(\frac{\varepsilon_2}{\varepsilon_p}\right)^2\right]d\varepsilon_2 \tag{16}$$

For $\varepsilon_{2s} > \beta\varepsilon_O$

$$K_1\beta f_c^{`} = \frac{A_1 + A_2}{\varepsilon_{2s}} = \frac{1}{\varepsilon_{2s}}\left(\int_0^{\varepsilon_{2S}} \beta f_c^{'}\left[2\left(\frac{\varepsilon_2}{\varepsilon_p}\right) - \left(\frac{\varepsilon_2}{\varepsilon_p}\right)^2\right]d\varepsilon_2 + \int_{\varepsilon_P}^{\varepsilon_{2s}}\left[1 - \left(\frac{\varepsilon_2 - \varepsilon_p}{2\varepsilon_0 - \varepsilon_p}\right)^2\right]d\varepsilon_2\right) \tag{17}$$

Where $A_o$, and $A_1$, $A_2$ are the shaded areas under ascending and descending portions of the softened stress – strain curve as shown in Fig. 12. $\varepsilon_1$ is the principal tensile strain of strut, $\varepsilon_l$ is the tensile strain of the longitudinal steel.

4th: Studying compatibility equations for each face of the space truss. Five basic equations are derived by Hus [21]. The first equation relates the angle of rotation (θ*) to the shear distortion (γ) in the wall. The second and the third equations relate the shear distortion (γ) in the wall to the strains in the tensile strain in the longitudinal reinforcement ($\varepsilon_l$) and the tensile strain in the stirrups ($\varepsilon_t$). The last two Eqs. (21) and (22) describe the bending of the concrete struts. The curvature of the diagonal concrete struts (ψ) is related to the angle of rotation (θ*) as expressed in Eq. (21). The last Eq. (22) relates the compressive surface strain, $\varepsilon_{2s}$ with the curvature of the concrete strut, ψ and the effective width of shear flow zone, $t_e$. Fig. 13 shows the total width of the thin-walled tube of softened space truss (t) due the bending of concrete struts, only the compression zone with effective width $t_e$ is considered. The strain distribution is assumed to be linear within the effective width of shear flow zone ($t_e$).

$$\theta^* = \frac{P_h\gamma}{2A_O} \tag{18}$$

$$\frac{\gamma}{2} = (\varepsilon_l + \varepsilon_2)\cot\theta \tag{19}$$

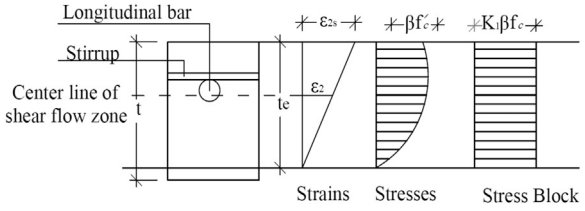


**Fig. 13.** The strain and stress distribution in the thin-walled tube of softened space truss [24].

$$\frac{\gamma}{2} = (\varepsilon_t + \varepsilon_2)\tan\theta \quad (20)$$

$$\Psi = \theta^*\sin 2\theta \quad (21)$$

$$\varepsilon_{2s} = \Psi t_e \quad (22)$$

5th: Studying the relationship between equilibrium and compatibility equations. The angle of rotation can be derived by using some trigonometric relationships together with the compatibility equations. The angle of rotation can be obtained as function of the compressive surface strain, effective thickness of shear flow zone($t_e$), and the inclination angle of the diagonal concrete struts (θ).

$$\theta^* = \frac{P_h}{A_o}(\varepsilon_t + \varepsilon_2)\tan\theta \quad (23)$$

$$\Psi = \frac{P_h}{A_o}(\varepsilon_t + \varepsilon_2)\tan\theta\sin 2\theta \quad (24)$$

$$\varepsilon_{2s} = \frac{2P_h t_e}{A_o}(\varepsilon_t + \varepsilon_2)\tan\theta\sin\theta\cos\theta \quad (25)$$

$$\theta^* = \frac{\varepsilon_{2s}}{2t_e\sin\theta\cos\theta} \quad (26)$$

### 4.2. Procedure of the proposed analytical model

The proposed model using excel sheet has been performed for nonlinear analysis of flanged RC beams subjected to pure torsion to calculate the torque (T) and the angle of twist (θ*). Fig. 14 presents the flow chart for the proposed theoretical model. The procedure can be summarized as follows:

Step (1): Select a value of the compressive strain at the surface of concrete strut $\varepsilon_{2s}$ where the maximum value of $\varepsilon_{2s}$ doesn't exceed 0.0035.
Step (2): Assume the angle of inclination of the diagonal concrete struts (θ = 45°) and calculate β from Eq. (13).
Step (3): Calculate the values of $A_{oh}$, $A_o$, $P_h$, and $t_e$ from Eqs. (5), (6), (7), (8) and (2), (3) (4), (8) for top and bottom chord of the beam respectively.
Step (4): Calculate $k_1$ from Eqs. (16) and (17) or from Table 3 then calculate $f_{cd}$ from equation (15).
Step (5): Calculate the torque for the top and the bottom chord, also calculate the corresponding angle of rotation θ * from Eqs. (10) and (26), respectively.
Step (6): Repeat the pervious steps with another value for $\varepsilon_{2s}$, consequently seven values for torque and corresponding angle of rotation and the torque- rotation curve can be plotted.

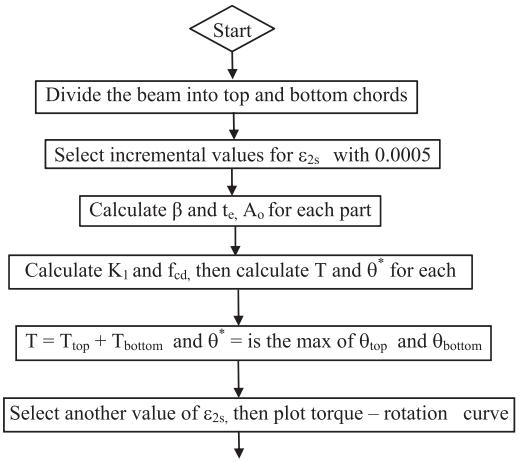


**Fig. 14.** Flow chart for calculating torque (T) and rotation angle (θ*).

**Table 3**
The value of $K_1$ corresponds to β and $\varepsilon_{2s}$ at all stages of loading [21].

| $\varepsilon_{2s}$ | 0.0005 | 0.001 | 0.0015 | 0.002 | 0.0025 | 0.003 | 0.0035 |
|---|---|---|---|---|---|---|---|
| β | $k_1$ | | | | | | |
| 0.1 | 0.8654 | 0.9215 | 0.9218 | 0.8994 | 0.861 | 0.8089 | 0.7439 |
| 0.2 | 0.7333 | 0.8611 | 0.8883 | 0.8806 | 0.8513 | 0.8048 | 0.7429 |
| 0.3 | 0.6018 | 0.798 | 0.8526 | 0.8604 | 0.8409 | 0.8005 | 0.7419 |
| 0.4 | 0.4948 | 0.7331 | 0.8147 | 0.8385 | 0.8294 | 0.7956 | 0.7407 |
| 0.5 | 0.4167 | 0.6667 | 0.7747 | 0.8148 | 0.8167 | 0.7901 | 0.7394 |
| 0.6 | 0.3588 | 0.6019 | 0.7325 | 0.7891 | 0.8026 | 0.784 | 0.7379 |
| 0.7 | 0.3146 | 0.5442 | 0.6889 | 0.7613 | 0.787 | 0.7771 | 0.7362 |
| 0.8 | 0.2799 | 0.4948 | 0.6445 | 0.7314 | 0.7698 | 0.7693 | 0.7432 |
| 0.9 | 0.2521 | 0.4527 | 0.6018 | 0.6997 | 0.7506 | 0.7603 | 0.7319 |
| 1.00 | 0.2292 | 0.4167 | 0.5625 | 0.6667 | 0.7292 | 0.75 | 0.7292 |

where, $\varepsilon_{2s}$ is the compressive strain at the surface of concrete strut at different stages of loading which doesn't exceed 0.0035, $k_1$ is the ratio between average stress ($f_{cd}$) and peak stress ($\beta f_c'$);and β is the concrete softening parameter.

### 4.3. Comparison of experimental and analytical results

The analytical and experimental torque-rotation curves of the specimens tested by the authors are shown in Fig. 15. All these specimens are with openings expect the control specimen $B_1$. The analytical torque-rotation curves predicted by the proposed model were validated by comparing the predicted and experimental curves of the seven specimens tested by the authors. Fig. 15 shows that the analytical torque-rotation curves predicted by the proposed model agrees well with the experimental ones.

## 5. Conclusions

The paper presents a test setup capable of simulating the behavior of reinforced concrete T- shaped beams under pure torsion. The torsional behavior of beams with and without rectangular web opening is investigated and the main conclusions drawn are summarized as follows:

1. The first cracks appeared at the two diagonal corners of web opening with 45- degree inclination to the longitudinal axis of the beams. The crushing of concrete was the main cause of the failure mode in all the tested beams. The crushing of the concrete was observed at the four corners of the openings
2. The geometrical parameters of beam flange have a great effect on the behavior of T-shaped beams under pure torsion. Increasing the flange width or flange thickness increases the torsional capacity and angle of rotation at different levels due to stiffness enhancement.
3. The increase of flange width by about 67%, increases the torsional capacity by 22% at the first crack level and by 10% at the ultimate level. Also, the angle of rotation is increased by 43% at the first crack level and 29% at the ultimate level.
4. When the flange thickness is increased by 50%, the torsional capacity is increased by 108% at the first crack level and by 33% at the ultimate level. Also, the angle of rotation is increased by 83% at first crack level and by 14% at the ultimate level.
5. The opening height affects the torsional capacity as it reduces the stiffness of the beam. When the opening height was doubled, the torsional capacity is decreased by 38.18% at the first crack level, and by 16% at the ultimate level. Also, the angle of rotation is decreased by 44% at the first crack level and by 17% at the ultimate level.
6. The proposed analytical model is reliable for predicting the torsional behavior of T- shaped RC beams with large web opening subjected to pure torsion where the model prediction agrees well with the experimental results.

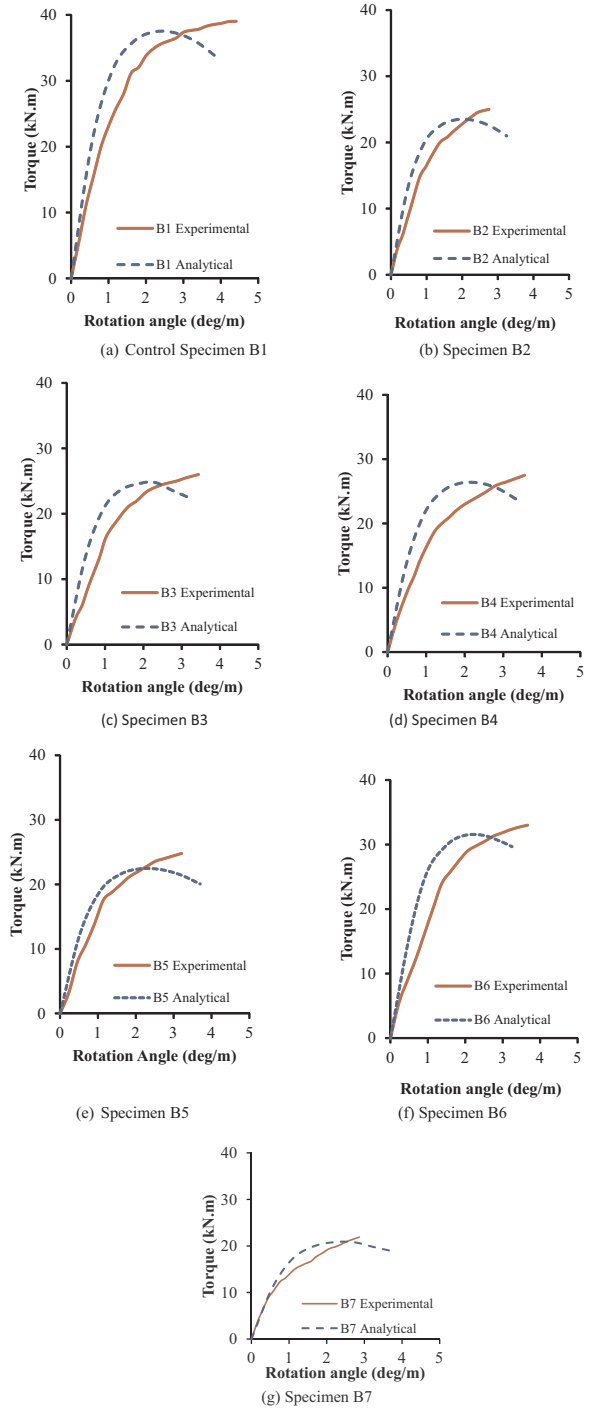


**Fig. 15.** Comparison between experimental and analytical torque-rotation curves.

## Appendix A. Supporting information

Supplementary data associated with this article can be found in the online version at http://dx.doi.org/10.1016/j.jobe.2018.02.004.

## References

[1] M. Mansur, K.H. Tan, Concrete beams with openings: analysis and design, CRC Press LLC, Boca Raton, Florida, USA, 1999, pp. 133–220.
[2] M. Mansur, S. Ting, S. Lee, Torsion tests of RC beams with large openings, J. Str. Div., ASCE. 109 (1983) 1780–1791.
[3] A. Abul Hasnat, F. Faisal, Wafa, A. Ali, Pre-stressed concrete beams with a small opening under torsion, ASCE J. 114 (1988) 1626–1643.
[4] A. Abd El Salam, Web Opening Effect on the Torsional Resistance of Reinforced Concrete Beams (M.Sc. Thesis), faculty of engineering, Benha University, Benha, Egypt, 2013.
[5] A. Salama, Behavior of Flanged Concrete Beams with Web Opening Under Pure Torsion (M.Sc. Thesis), Faculty of Engineering, Cairo University, Cairo, Egypt, 2014.
[6] M. Mansur, Effect of openings on the behavior and strength of RC beams in shear. cement conc, Comp (1998) 477–486.
[7] K. El Badry, Behavior of high strength concrete beams with web opening subjected to torsion (Ph.D. Thesis), dept. of str. Eng., Cairo Univ., Egypt, 2003.
[8] A. Deifalla, A. Ghobarah, Behavior and analysis of inverted T-shaped RC beams under shear and torsion, Eng. Str. J. 68 (2014) 57–70.
[9] A. Deifalla, A. Ghobarah, Simplified analysis of RC beams torsionaly strengthened using FRP, BBFS (2005) 381–386.
[10] A. Deifalla, Behavior and strengthening of RC T-girders in torsion and shear, Ph.D. thesis, McMaster University, Canada, (2007).
[11] A.A. Ewida, A.E. McMullen, Torsion–shear–flexure interaction in reinforced concrete members, Mag. Conc. Res. 23 (1981) 113–122.
[12] E. Rausch, Design of Reinforced Concrete in Torsion, E. Rausch Ph.D. Thesis, Berlin, 1952., Berlin, 1952.
[13] G. Greene Jr., A. Belarbi, Model for reinforced concrete members under torsion, bending, and shear, I: Theory, J. Eng. Mech. 135 (2009) 961–969.
[14] K.N. Rahal, M.P. Collins, Analysis of sections subjected to combined shear and torsion - A theoretical model, ACI Str. J. 92 (1995) 459–469.
[15] L.F.A. Bernardo, J.M.A. Andrade, S.M.R. Lopes, Behavior of concrete beams under torsion – NSC plain and hollow beams, Mat. Str. J. 41 (2008) 1143–1167.
[16] L.H. Huang, Y. Lu, C. Shi, Unified calculations method for symmetrically reinforced concrete section subjected to combined loading, ACI Str. J. 110 (2013) 127–136.
[17] M. Kaminski, W. Pawlak, Load capacity and stiffness of angular cross section reinforced concrete beams under torsion, Arch. Civil. Mech. Eng. XI (2011) 885–903.
[18] M.P. Collins, D. Mitchell, Shear and torsion design of pre-stressed and non- pre-stressed concrete beams, Pci. J. 25 (1980) 32–100.
[19] L.F.A. Bernardo, J.M.A. Andrade, S.M.R. Lopes, Modified variable angle truss-model for torsion in reinforced concrete beams, Mater. Str. 45 (2012) 1877–1902.
[20] L.F.A. Bernardo, J.M.A. Andrade, S.M.R. Lopes, Softened truss model for reinforced NSC and HSC beams under torsion: a comparative study, Eng. Str. 42 (2012) 278–296.
[21] T.C. Hsu, Y.L. Mo, Softening of concrete in torsional members - theory and tests, ACI J. Proc. 82 (1985) 290–303.
[22] K.N. Rahal, M.P. Collins, Simple model for predicting torsional strength of reinforced and Prestressed concrete sections, ACI Str. J. 93 (1996) 658–666.
[23] ACI Committee 318, Building Code Requirements for Structural Concrete (ACI 318-14), American Concrete Institute, Detroit, Michigan, USA, 2014.
[24] Canadian Standards Association CSA standard (A23.3-14), Design of Concrete Structures for Buildings, Rexdale, Ontario, Canada, 2014.
[25] ECP 203-2009, Egyptian Code for Design and Construction of Concrete Structures, Ministry of building construction, Research center for housing, Building and physical planning, Cairo, Egypt, 2009.
[26] A. Deifalla, A. Awad, M. El-Garhy, Effectiveness of externally bonded CFRP strips for strengthening flanged beams under torsion: an experimental study, Eng. Str. J. 56 (2013) 2065–2075.
[27] A. Deifalla, A. Ghobarah, Full torsional behavior of RC beams wrapped with FRP: analytical model, ASCE, Comp. Constr. 14 (2010) 289–300.
[28] A. Deifalla, A. Ghobarah, Strengthening RC T-Beams subjected to combined torsion and shear using FRP fabrics – Experimental study, ASCE Comp. Constr. 14 (2010) 301–311.
[29] M. Ghoneim, M. El-Mihilmy, Design of Reinforced Concrete Structures, fourth ed., Vol.1, 2014.
[30] ACI Committee 318, Building Code Requirements for Structural Concrete (ACI 318-89), American Concrete Institute, Detroit, Michigan, USA, 1989.
[31] ACI Committee 318, Building Code Requirements for Structural Concrete (ACI 318-99), American Concrete Institute, Detroit, Michigan, USA, 1999.
[32] E. Morsch, Concrete-Steel Construction, third ed., McGraw-Hill book Company, New York, 1909.
[33] F.J. Vecchio, M.P. Collins, Compression response of cracked reinforced concrete, ASCE Str. J. 119 (1993) 3590–3610.
[34] F.J. Vecchio, M.P. Collins, Stress-strain characteristics of reinforced concrete in pure torsion, IABSE Colloq. Adv. Mech. Reinf. Conc. (1981) 211–225.
[35] F.J. Vecchio, M.P. Collins, The modified compression field theory for reinforced concrete elements subjected to shear, ACI Str. J. 83 (1986) 219–231.
[36] F.J. Vecchio, M.P. Collins, The response of reinforced concrete to in-plane shear and normal stresses 82 Department of civil engineering, Toronto univ., 1982, p. 332.